Pis'ma v ZhETF, vol. 96, iss. 7, pp. 484 – 491

Giant Rashba-type spin splitting at polar surfaces of BiTeI

S. V. Eremeev[+*1)], *I. A. Nechaev*[*×], *E. V. Chulkov*[×∇]

[+] *Institute of Strength Physics and Materials Science SB RAS, 634021 Tomsk, Russia*

[*] *Tomsk State University, 634050 Tomsk, Russia*

[×] *Donostia International Physics Center, 20018 San Sebastián, Basque Country, Spain*

[∇] *Departamento de Fisica de Materiales UPV/EHU, 20080 San Sebastián, Basque Country, Spain*

Submitted 1 August 2012

On the basis of relativistic *ab-initio* calculations, we show that both Te- and I-terminated surfaces of the polar layered semiconductor BiTeI hold surface states with a giant Rashba-type spin splitting. The Te-terminated surface state has nearly isotropic free-electron-like dispersion with a positive effective mass, which along with the giant spin splitting makes BiTeI fulfilling the requirements demanded by many semiconductor-spintronics applications. The I-terminated surface state with its negative effective-mass dispersion reproduces nicely the situation with the Rashba-split surface state on surfaces of noble-metal based surface alloys. The crucial advantage of BiTeI as compared with the surface alloys is the location of the I-terminated surface state in a quite wide band gap.

Nowadays, there is a growing demand for real materials that in addition to their ease of processing exhibit a giant spin-orbit Rashba-type spin splitting of a free-electron-like surface state at a semiconductor surface. Such a demand is caused by the fact that these materials can provide a basis for many theoretically proposed spintronics devices. Actually, in a two-dimensional ($2D$) electron system formed by surface-state electrons the Rashba spin splitting [1] gives an opportunity of controllable spin manipulation via an applied electric field [2–4]. At that large magnitude of the splitting and high carrier mobility caused by a metallic-like surface-state dispersion make a surface spin signal detectable even at room temperature.

The well-known conventional semiconductor structures [4–6] possess $2D$ electron systems that are characterized by an essentially small spin splitting due to weak spin-orbit interaction (SOI). Significantly greater spin splitting of $2D$ electron states has been found in a system formed by surface-state electrons in Bi and noble-metal-based Bi-surface alloys [7–11]. However, in this case one deals with a metallic substrate that prevents tuning of the spin splitting by external electric field and introduces the large bulk current into a surface spin signal. This fact has inspired a renewed interest in semiconductors with strong spin-orbit interaction. In order to advance in the search of a semiconductor-based $2D$ system with large spin-splitting and ease of processing, we consider surface electronic structure of BiTeI. Our interest in this material has been triggered by recently published results on spin- and angle-resolved photoemission spectroscopy (ARPES) measurements, which have revealed a giant Rashba-type [12, 13] spin splitting of bulk states in this polar semiconductor.

In this paper, we present a theoretical *ab initio* study of Te- and I-terminated (0001) surfaces of BiTeI, which due to the pronounced three-layered (TL) crystal structure can naturally appear under cleavage. We show that at both surfaces, Te- and I-terminated, the spin-orbit-split surface states emerge by splitting off from the bulk conduction or valence band. These states inherit their Rashba-type spin splitting and spin structure from the respective bulk states.

For structural optimization and electronic band calculations, we employed density functional theory (DFT) with the generalized gradient approximation (GGA) [14] for the exchange-correlation (XC) potential as implemented in VASP [15, 16]. The interaction between the ion cores and valence electrons was described by the projector augmented-wave method [17, 18]. The Hamiltonian contained the scalar relativistic corrections, and the spin-orbit coupling was taken into account by the second variation method [19].

The polar layered semiconductor BiTeI has a hexagonal crystal structure (space group $P3m1$) [20] (Fig. 1a), formed by Bi, Te, and I layers stacked along the c-axis. This semiconductor is characterized by ionic bonding and the mentioned TL structure, where the distance between TLs is about one and a half times greater than those within the Te-Bi-I TL.

In Fig. 1c, we show the calculated bulk band structure. The obtained electronic bands are in good agree-

[1)] e-mail: eremeev@ispms.tsc.ru

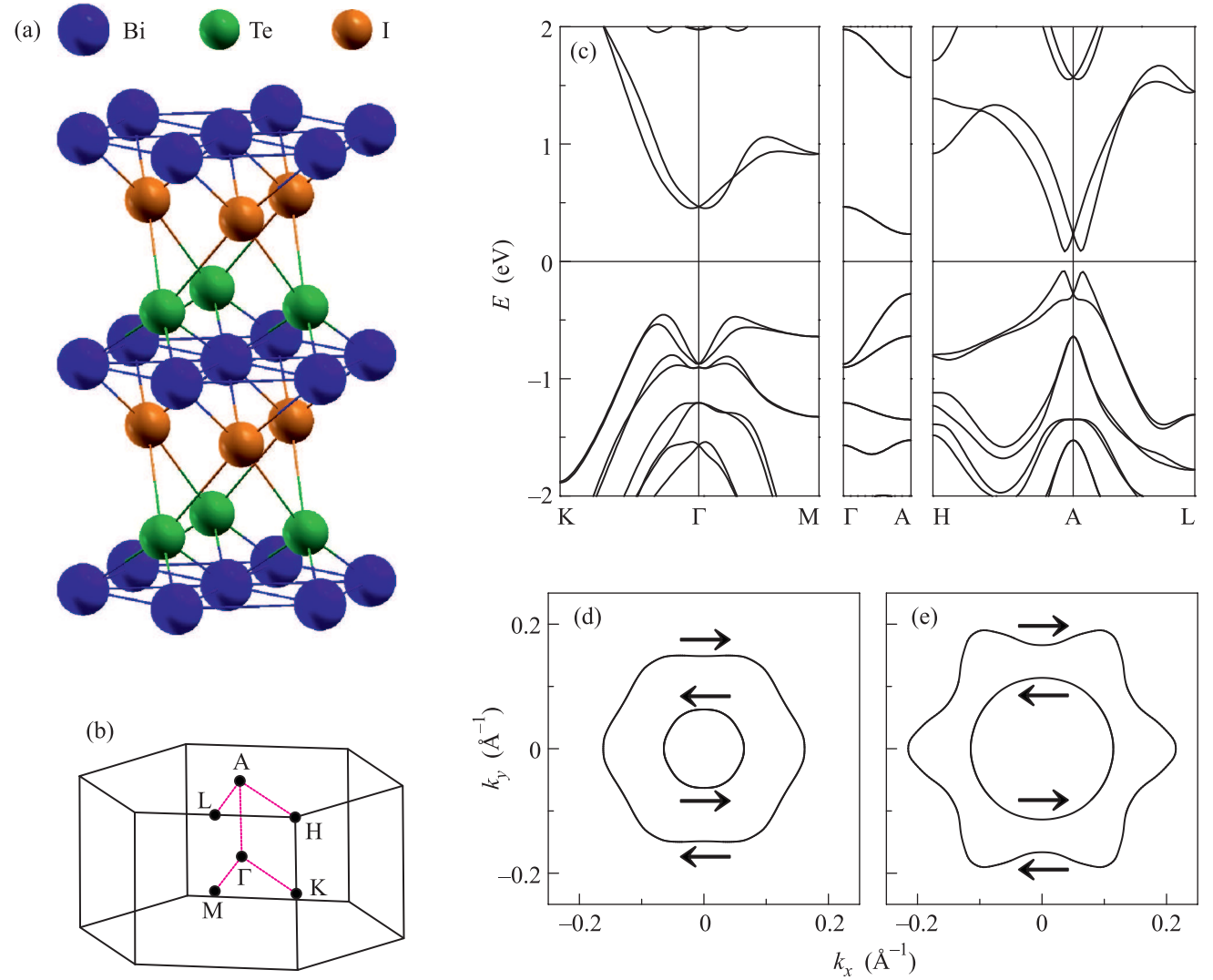

Fig. 1. (Color on-line) Atomic crystal structure (a), Brillouin zone (b), and bulk BiTeI electronic structure calculated along high symmetry directions of the Brillouin zone. Constant energy contours for conduction (d) and valence (e) bands in the vicinity of the A point at 250 meV above (d) and at 80 meV below (e) the band degeneracy point. In panels (d) and (e) arrows show spin directions

ment with FLAPW calculations [12, 21, 22]. As is clearly seen in the figure, both the conduction band minimum (CBM) and the valence band maximum (VBM) demonstrate giant Rashba-type spin splitting in $2D$ (k_x, k_y)-planes perpendicular to the $\Gamma - A$ direction. To describe this splitting in the Rashba-model terms, we would remind that SOI shifts opposite spin polarized $2D$ electron bands by the momentum k_{R} in opposite directions. The resulting splitting is characterized by the energy E_{R} and coupling parameter $\alpha_{\mathrm{R}} = 2E_{\mathrm{R}}/k_{\mathrm{R}}$. In the vicinity of the A point, where one can find the biggest spin spitting, $k_{\mathrm{R}} \approx \pm 0.055\,\text{Å}^{-1}$ for the CBM and $k_{\mathrm{R}} \approx \pm 0.060\,\text{Å}^{-1}$ for the VBM. The values of the coupling parameter α_{R} for the CBM in the AH and AL directions are 5.26 and 5.33 eV·Å^{-1}, respectively. Our α_{R} for the CBM is slightly larger than that obtained in Refs. [12, 21]. We attribute it mainly to the larger E_{R}. The values of α_{R} for the VBM are larger than those for the CBM. They are 6.08 and 6.55 eV·Å^{-1} for the AH and AL directions, respectively.

The constant energy contours (CEC) (shown in Fig. 1d) demonstrate a circular shape for the inner branch and a hexagonal shape for the outer branch of the spin-split conduction band. The deviation of the outer-branch CEC from the circular shape is accompanied by the sizeable out-of-plane spin component S_z, while for the circular inner branch S_z component is significantly smaller. This feature is in agreement with the calcu-

lated CEC for the conduction band given in Ref. [12]. The CEC for the valence band (Fig. 1e) shows a more warped shape for the outer branch, which is accompanied by the larger out-of-plane spin component. In contrast to the non-zero in-plane spin component that appears due to the potential gradient in z-direction, the out-of-plane component is caused by an in-plane potential gradient (see, e.g., Refs. [8] and [23]). At that, the larger the in-plane gradient that corresponds to the state localization, the stronger the anisotropy of the respective energy dispersion we have. In spite of the marked difference, the Rashba-split valence band has the same spin helicity as the conduction band, i.e. clockwise spin rotation in the outer branch and counter-clockwise one in the inner branch.

The surface of BiTeI formed under cleavage can have two possible terminations: Te- or I-layer. To simulate semi-infinite BiTeI(0001) with Te-terminated surface, we consider a 8 TL slab with iodine side passivated by hydrogen monolayer. The electronic band spectrum of this slab is shown in Fig. 2a, where the size of the black and light gray circles is proportional to weights of the states localized on Te- and H-I-side of the slab, respectively. As seen in the figure, at the Te-terminated surface the spin-orbit-split surface state arises in the energy gap just below the conduction band. The charge density of this surface-state is localized in the two topmost TLs (Fig. 2b) and has the spin-splitting characterized by $\alpha_{\mathrm{R}} \approx 3.5\,\mathrm{eV}\cdot\text{Å}$ which is two times larger than that recently reported for the surface state in BiTeCl [22].

The emergence of the surface state can be understood from analysis of changes of the near-surface potential. The break of translational symmetry along the c-axis in the strong ionic system leads to considerable modification of the electrostatic potential near the surface. In Fig. 2c, the change ΔV of the local potential averaged over (xy)-plane with respect to that in the central part of the slab is shown as a function of z. The position of $z = 0$ corresponds to the plane of the topmost Te atomic layer. The pronounced TL structure of the compound produces stepwise behaviour of ΔV. The largest decrease of the potential is in the outermost TL, while in the third TL it becomes negligible. This change in the potential in the vicinity of the surface reflects trapping of electrons of the outermost TL, which splits off the spin-split state from the bulk conduction band and noticeably increases its effective mass. The found modifications of the potential within the outermost TL also lead to decrease of the strength α_{R}.

It was experimentally shown that in BiTeI the CECs have circular shape for both inner and outer branches at the Fermi level, which lies at 0.29 eV above the band bottom. Fig. 2d shows that the calculated CECs for the surface state at the same energy are in good agrement with the experimental data. It should be noted that the outer-branch CEC, being hexagonal in the case of the bulk CBM (see Fig. 1d), becomes circular-like for the surface state that splits off from the bulk conduction band. It reflects a decrease of the in-plane potential gradient in the topmost TL as compared with that in the bulk BiTeI. As to the in-plane spin helicity of the surface state, the in-plane spin texture is inherited from the bulk conduction band. The expectation value of the out-of-plane spin component S_z is zero along $\bar{\Gamma} - \bar{\mathrm{M}}$ owing to symmetry constrains, and it has maximal value along $\bar{\Gamma} - \bar{\mathrm{K}}$ at any chosen energy. In Fig. 2e we show absolute value of the S_z as a function of $k_{\bar{\mathrm{K}}}$ for the inner and outer branches of the spin-split surface state. As one can see, for small $k_{\bar{\mathrm{K}}}$, i.e. below the bulk conduction band minimum, $|S_z|$ is negligibly small and thus, the surface state is completely in-plane spin polarized. With increasing $k_{\bar{\mathrm{K}}}$, $|S_z|$ for the outer branch increases smoothly and already at $k_{\bar{\mathrm{K}}} \sim 0.3\ \text{Å}^{-1}$ gets some "saturation", whereupon $|S_z|$ remains practically unchanged. For the inner branch, $|S_z|$ demonstrates more complicated behavior. The reason for this behavior may be due to the fact that just above the degeneracy point the inner branch enters the bulk states region. As was shown [24, 25], the spin split bulk continuum states demonstrate beating of the spin density near the surface. The hybridization of the inner branch of the surface state with the spin-split bulk states may cause the surface state acquiring such a beating.

As seen in Fig. 2a, within a wide energy interval the calculated surface-state dispersion can be fitted properly to the Rashba-model spin-orbit-split $2D$ electron state. It is worth noting that the resulting model dispersion, in turn, is in good agreement with the ARPES measurements of Ref. [12], as is demonstrated in Fig. 3a. This fact allows us to go further than merely describing the DFT results. Actually, with the use of the G_0W_0 scheme of Ref. [26] based on the Rashba model (see also Refs. [22, 27]), we can gain an insight into quasiparticle dynamics at the Te-terminated surface of BiTeI. We suppose that we deal with the $2D$ Rashba-spin-orbit coupled electron gas with $m^* = 0.1489\,m_e$ and $\alpha_{\mathrm{R}} = 3.5\,\mathrm{eV}\cdot\text{Å}$, which is immersed in the medium with the dielectric constant $\varepsilon_\infty = 19 \pm 2$ [?] of the bulk BiTeI. We consider two values of the $2D$ charge density, which correspond to two locations of the Fermi level shown in Fig. 3a. Since the Fermi level can be tuned by, e.g., doping or electric field, the considered locations can be realized in practice.

In Fig. 3b, the quasiparticle lifetime and decay rate caused by inelastic electron-electron scattering in the

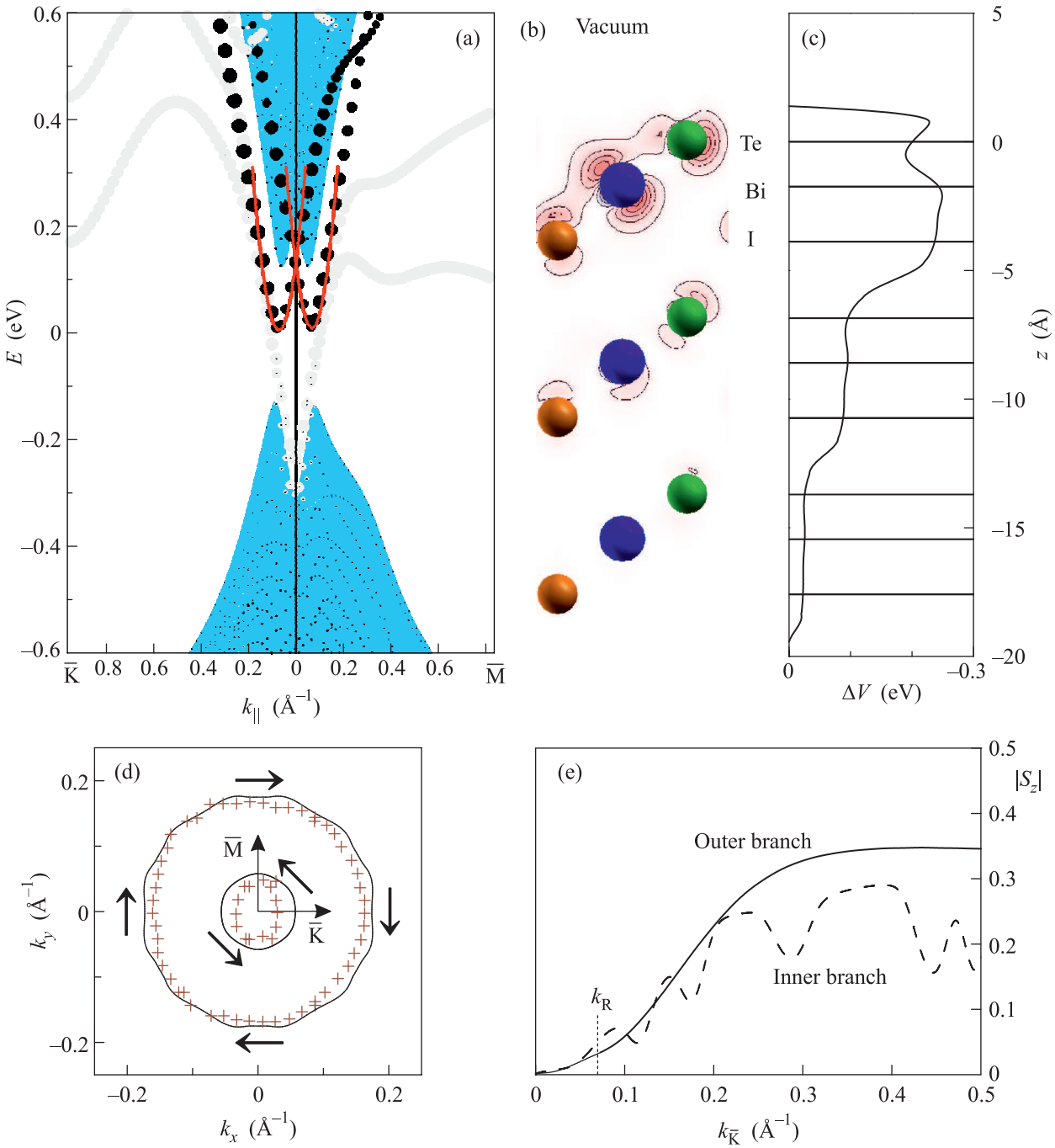

Fig. 2. (Color on-line) Electronic structure of Te-terminated BiTeI(0001). (a) – Band structure of a 8 TL slab with hydrogen on the I-terminated side (the black (gray) bands are states from the outermost TL of the Te(H)-terminated side of the slab, shaded area is the bulk states, red curves are parabolic Rashba-model fitting, zero energy corresponds to the middle of the bulk gap). (b) – Spatial distribution of the $\bar{\Gamma}$-surface-state charge density in the $(11\bar{2}0)$ plane. (c) – The change of the potential in near-surface layers with respect to that in central layers (horizontal lines show position of atomic layers). (d) – Constant energy contours for Rashba split surface states at energy of 0.29 eV above the band bottom. Arrows show the in-plane spin directions, crosses are experimental data taken from Ref. [12]. (e) – Out-of-plane spin component S_z traced along the $\bar{\Gamma} - \bar{\mathrm{K}}$ direction

mentioned $2D$ electron gas are presented for the Fermi level located above the energy E_0 that corresponds to the branch-crossing point at $k_{||} = 0$. First, we would like to note that the quasiparticle lieftime τ is mainly within time domain of a few picoseconds. There is a slight difference between τ for the inner and the outer branch,

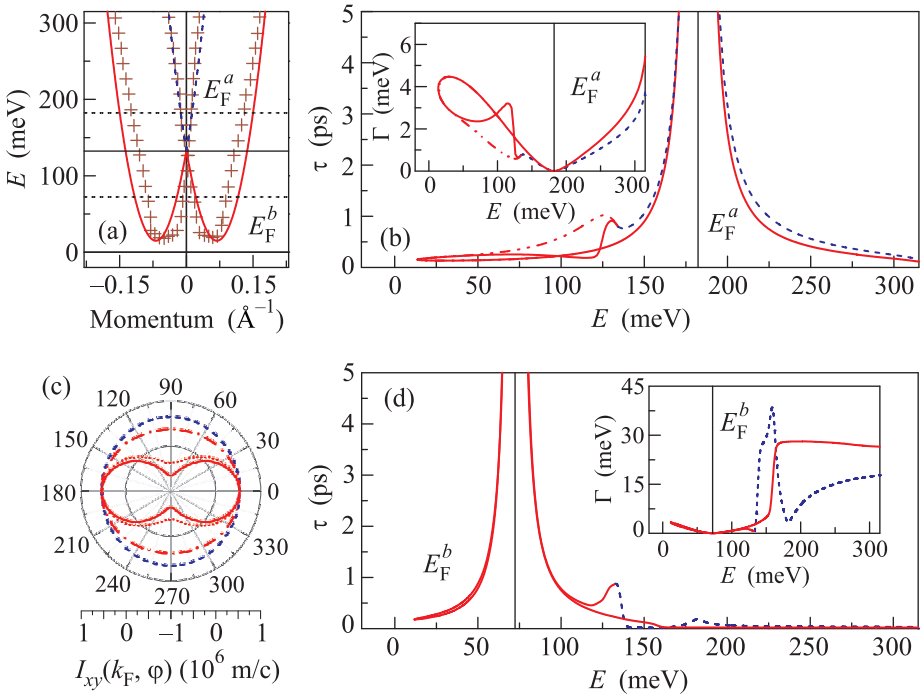

Fig. 3. (Color on-line) Surface-state quasiparticle dynamics at the Te-terminated surface of BiTeI. (a) – The parabolic Rashba-model fitting. Crosses are experimental data of Ref. [12]. Dashed horizontal lines indicate two Fermi energies ($E_F^a = 50$ meV and $E_F^b = -60$ meV as measured from the degeneracy point E_0). (b) – The inelastic quasiparticle lifetime τ and decay rate Γ (see the inset) for the inner (dashed lines) and the outer (solid lines) branch in the E_F^a case. Dash-dot-dotted lines show τ and Γ without the plasmon decay-channel contribution at energies less than E_0. (d) – Polar plot of the contribution I_{xy} to the spin current at the Fermi momenta k_F as a function of the angle φ ($\varphi = 0$ corresponds to the k_x direction). In the E_F^a case, the inner and the outer branches are presented by dashed and solid lines, respectively. The E_F^b case is characterized by two loops of the outer branch for the smaller (dash-dotted line) and the bigger (dotted line) Fermi momentum. (d) – The same as in panel (b), but in the E_F^b case

which along with equal velocities for both branches at a given energy leads to respective difference in the inelastic mean free path. Second, below E_0, where only outer branch exists, one can see a loop with a hump that is caused by opening the plasmon-emission channel for holes (see the inset in Fig. 3b). This plasmon-related feature may disappear, when the bulk conduction band in the considered excitation-energy region will be involved in screening-property calculations.

Within the Rashba-model, we can also estimate the spin current in the $2D$ electron system formed by Te-terminated surface-state electrons. According to the definition of Ref. [29], which has been reproduced within more general consideration of Ref. [30], the spin current tensor $\mathcal{J}_{ij} = \sum_s \int d\mathbf{k} f_{\mathbf{k}}^s I_{ij}^s(\mathbf{k})/(2\pi)^2$ is obtained by summation of the contribution $I_{ij}^s(\mathbf{k}) = \langle \psi_{s\mathbf{k}} | \sigma_i v_j + v_j \sigma_i | \psi_{s\mathbf{k}} \rangle / 2$ over all occupied states $\psi_{s\mathbf{k}}$ of the inner ($s = +$) and the outer ($s = -$) branch. Here, σ_i and $f_{\mathbf{k}}^s$ are the Pauli matrices and the Fermi distribution function, respectively, and v_j are components of the operator of the velocity. In our case, the tensor is antisymmetric with nonzero components $\mathcal{J}_{xy} = -\mathcal{J}_{yx}$. The contributions $I_{xy}^s(k_F^s, \phi)$ coming from the states at the Fermi energy E_F^a are shown in Fig. 3c. As one can see, along the y-axis ($\varphi = 90°$) there is a compensation of the contributions from different branches, whereas with φ swinging from the y-axis a sum of the contributions can lead to net macroscopic spin current. For the system under study, the resulting spin current $\mathcal{J}_{xy}$ can exceed its value in, e.g., InAs-based semiconductor quantum wells by about four orders of magnitude.

Due to the revealed giant spin-splitting of the surface state, a situation with the Fermi level that lies in the energy region, where only the outer branch is populated, becomes feasible in practice. Fig. 3d reflects behaviour of τ and Γ in such a situation. In the energy region that does not contain bulk-projected states ($E_F^b \pm 60$ meV) and, therefore, corresponds to a more accurate description of quasiparticle dynamics within the Rashba-model-based G_0W_0 scheme, hole and electron excitations behave similar to the excitations in an ordinary $2D$ electron gas without the SOI. However, there

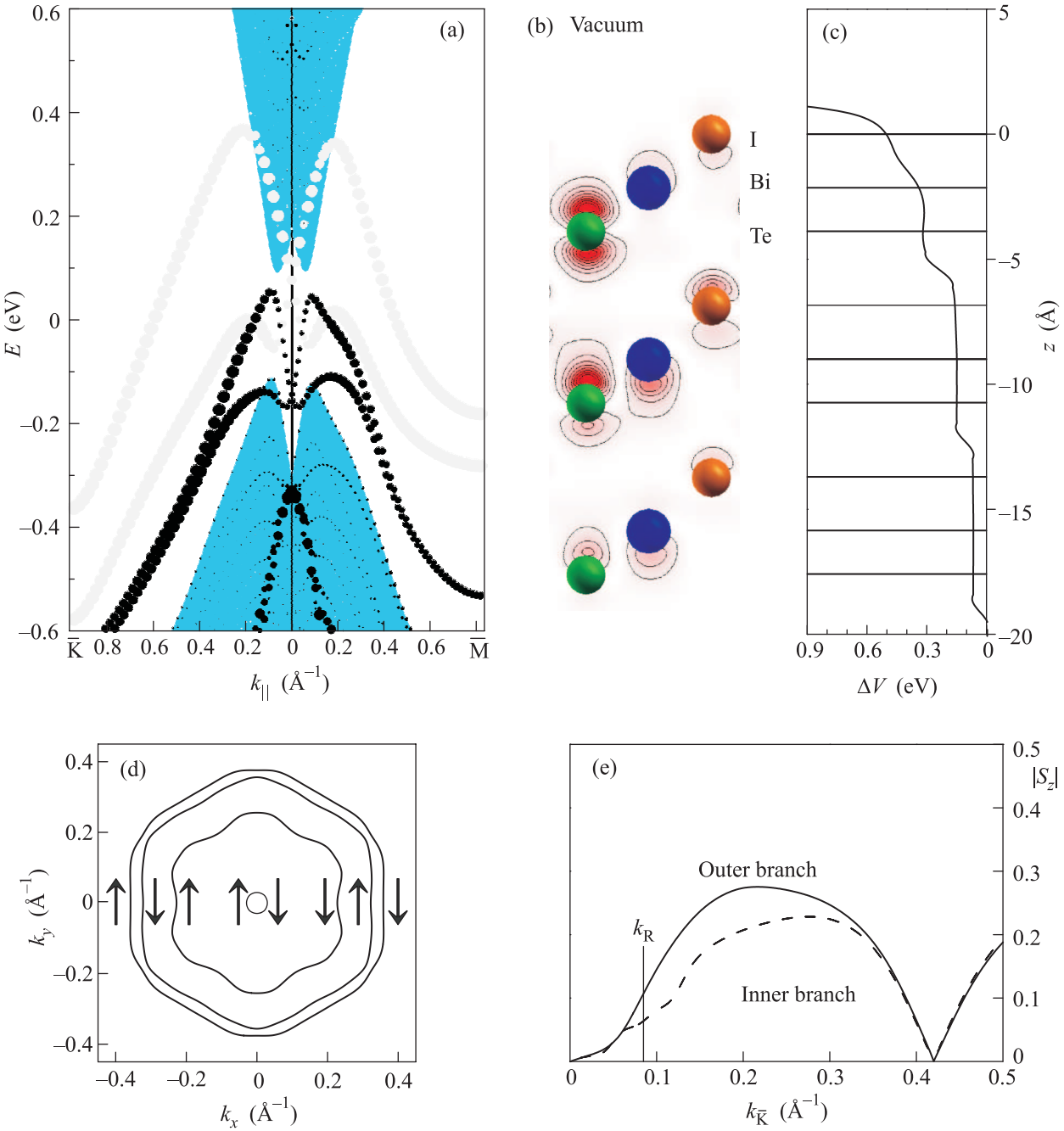

Fig. 4. (Color on-line) Electronic structure of I-terminated BiTeI(0001). (a) – Band structure of a 8 TL slab (the black bands are states from outermost TL of the I-terminated side of the slab). (b) – Spatial distribution of the $\bar{\Gamma}$ surface-state charge density in the $(11\bar{2}0)$ plane. (c) – The change of the potential in near-surface layers with respect to that in central layers. (d) – CECs for the VB Rashba-split surface states at energies of 80 meV below (solid lines) and above (dashed lines) the degeneracy point. Arrows show the in-plane spin directions. (e) – Out-of-plane spin component S_z traced along the $\bar{\Gamma} - \bar{K}$ line

is an important distinction that consists in the fact that here at a given direction of **k** carriers with only one spin orientation exist. Above the E_0 energy, the shown behavior of the lifetime is mainly driven by a contribution of the plasmon-decay channel that is unlikely to be observed, since, as was already mentioned, taking the bulk states into account can change screening properties of the considered system. As to the spin current, it still

can arise (see Fig. 3c), but the value becomes slightly smaller than in the E_F^a case.

Now we consider the I-terminated surface. It is simulated by 8 TL slab with passivated opposite side of the slab (here we use fluorine to passivate the Te-terminated surface). In contrast to the Te-terminated surface, on the I-terminated BiTeI(0001) surface a hole-like spin-split surface state resides in the bulk gap (Fig. 4a). This state is localized in the three upper TL's near the BZ center (Fig. 4b) while at $k_{||} \geq k_R$ it becomes strongly localized in the outermost TL. The surface state is formed owing to the positive bending of the potential near the surface (see Fig. 4c). The magnitude of the ΔV is larger than that on the Te-terminated surface. Such a ΔV provides larger split off of the valence band edge, so both branches of the surface state lie in the band gap (except for a small overlap of the inner branch with bulk states at $k_{\bar{K}} \approx 0.07\,\text{Å}^{-1}$). The CECs given for ± 80 meV below and above the degeneracy point in Fig. 4d show less pronounced anisotropy of the surface state with respect to $k_{||}$ than it is for the bulk valence state. As in the previous case, $|S_z|$ increases at small $k_{\bar{K}}$ but drops to zero at $0.42\,\text{Å}^{-1}$, where the inner and outer branches are swapped. This feature is inherited from the intersection of the upper bulk valence bands in the middle of $A - H$ direction (see Fig. 1c).

The spin-splitting of the I-terminated surface state is characterized by $k_R = 0.087$ and $0.082\,\text{Å}^{-1}$ in $\bar{\Gamma} - \bar{K}$ and $\bar{\Gamma} - \bar{M}$ direction, respectively, and E_R equal to 0.20 eV ($\bar{\Gamma} - \bar{K}$) and 0.19 eV ($\bar{\Gamma} - \bar{M}$). This characteristics yield $\alpha_R \approx 4.6\,\text{eV}\cdot\text{Å}^{-1}$, which significantly exceeds α_R at the Te-terminated surface and is 30–40 times larger than the currently known Rashba parameters in $2D$ electron systems of the traditional semiconductor structures. However, at the same time the obtained dispersion of the surface state cannot be adequately fitted to the Rashba model. As a consequence, in this case quasiparticle dynamics cannot be properly described within the G_0W_0 scheme used above. Nevertheless, the I-terminated surface electronic structure resembles that for the surface alloys with one crucial advantage: the present surface state resides in the wide bulk band gap.

In conclusion, we have shown that BiTeI polar surfaces possess surface states, which demonstrate the giant Rashba-type spin splitting. This splitting is inherited from that of the bulk bandgap edge states. The surface states emerge by splitting off from the lowest conduction (at the Te-terminated surface) or the uppermost valence (at the I-terminated surface) band, owing to the potential bending within the near-surface layers.

The Te-terminated surface state is an isotropic, the dispersion and the spin splitting of which can be well described within the Rashba model. This fact has allowed us to gain an insight into quasiparticle lifetimes and to estimate the spin current in the $2D$ system formed by electrons in the Te-terminated surface state. We have found that in the case of the Fermi level located in the energy range, where only the outer branch is populated, the lifetime is within time domain of a few picoseconds and demonstrates ordinary behavior as a function of excitation energy within the interval of ~ 120 meV. This case stands out also for quasiparticles that at a given momentum direction have only one spin orientation. The estimated spin current can exceed its value in conventional semiconductor quantum wells by about four orders of magnitude.

As compared with the Te-terminated surface, the I-terminated surface state that shows negative effective-mass dispersion has an advantage of a larger spin splitting and of a location of the state (predominantly by its outer branch) in the quite wide band gap of BiTeI.

We acknowledge partial support by the University of the Basque Country (project # GV-UPV/EHU, grant # IT-366-07) and Ministerio de Ciencia e Inovación (grant # FIS2010-19609-C02-00). Calculations were performed on SKIF-Cyberia (Tomsk State University) supercomputer.

1. E. I. Rashba, Sov. Phys. Solid State **2**, 1109 (1960); Y. A. Bychkov and E. I. Rashba, JETP Lett. **39**, 78 (1984); J. Phys. C **17**, 6039 (1984).
2. M. Studer, G. Salis, K. Ensslin et al., Phys. Rev. Lett. **103**, 027201 (2009).
3. S. Datta and B. Das, Appl. Phys. Lett. **56**, 665 (1990).
4. J. Nitta, T. Akazaki, H. Takayanagi, and T. Enoki, Phys. Rev. Lett. **78**, 1335 (1997).
5. G. Engels, J. Lange, T. Schäpers, and H. Lüth, Phys. Rev. B **55**, R1958 (1997).
6. D. Grundler, Phys. Rev. Lett. **84**, 6074 (2000).
7. Yu. M. Koroteev, G. Bihlmayer, J. E. Gayone et al., Phys. Rev. Lett. **93**, 046403 (2004).
8. C. R. Ast, J. Henk, A. Ernst et al., Phys. Rev. Lett. **98**, 186807 (2007).
9. G. Bihlmayer, S. Blügel, and E. V. Chulkov, Phys. Rev. B **75**, 195414 (2007).
10. C. R. Ast, D. Pacilé, L. Moreschini et al., Phys. Rev. B **77**, 081407(R) (2008).
11. H. Mirhosseini, J. Henk, A. Ernst et al., Phys. Rev. B **79**, 245428 (2009).
12. K. Ishizaka, M. S. Bahramy, H. Murakawa et al., Nature Materials **10**, 521 (2011).
13. G. Landolt, S. V. Eremeev, Yu. M. Koroteev et al., Phys. Rev. Lett. **109**, 116403 (2012).

14. J. P. Perdew, K. Burke, and M. Ernzerhof, Phys. Rev. Lett. **77**, 3865 (1996); J. P. Perdew, K. Burke, and M. Ernzerhof, Phys. Rev. Lett. **78**, 1396(E) (1997).
15. G. Kresse and J. Hafner, Phys. Rev. B **48**, 13115 (1993).
16. G. Kresse and J. Furthmüller, Comput. Mater. Sci. **6**, 15 (1996).
17. P. E. Blöchl, Phys. Rev. B **50**, 17953 (1994).
18. G. Kresse and D. Joubert, Phys. Rev. B **59**, 1758 (1999).
19. D. D. Koelling and B. N. Harmon, J. Phys. C **10**, 3107 (1977).
20. A. V. Shevelkov, E. V. Dikarev, R. V. Shpanchenko, and B. A. Popovkin, J. Solid State Chem. **114**, 379 (1995).
21. M. S. Bahramy, R. Arita, and N. Nagaosa, Phys. Rev B **84**, 041202(R) (2011).
22. S. V. Eremeev, I. A. Nechaev, Yu. M. Koroteev et al., Phys. Rev. Lett. **108**, 246802 (2012).
23. J. Premper, M. Trautmann, J. Henk, and P. Bruno, Phys. Rev. B **76**, 073310 (2007).
24. A. Kimura, E. E. Krasovskii, R. Nishimura et al., Phys. Rev. Lett. **105**, 076804 (2010).
25. E. E. Krasovskii and E. V. Chulkov, Phys. Rev. B **83**, 155401 (2011).
26. I. A. Nechaev and E. V. Chulkov, Phys. Solid State **51**, 1772 (2009).
27. I. A. Nechaev, V. M. Silkin, and E. V. Chulkov, JETP **112**, 134 (2011).
28. P. Lostak, J. Horak, A. Vasko, and T. D. Nguyen, Phys. Stat. Solidi A **59**, 311 (1980).
29. E. I. Rashba, Phys. Rev. B **68**, 241315(R) (2003).
30. I. V. Tokatly, Phys. Rev. Lett. **101**, 106601 (2008).